Dalton Transactions

Accepted Manuscript

ROYAL SOCIETY OF CHEMISTRY

www.rsc.org/dalton

Response surface methodology approach for optimization of simultaneous dyes and metal ions ultrasound-assisted adsorption onto Mn doped Fe_3O_4-NPs loaded on AC: Kinetic and isotherm study

Arash Asfaram [a], Mehrorang Ghaedi [*a], Alireza Goudarzi [b], Maryam Rajabi [c]

[a] *Chemistry Department, Yasouj University, Yasouj 75918-74831, Iran.*
[b] *Department of Polymer Engineering, Golestan University, Gorgan, 49188-88369, Iran*
[c] *Chemistry Department, Faculty of Science, Semnan University, Semnan 35195-363, Iran*

* Corresponding author at: Tel.: +98 741 2223048; fax: +98 741 2223048.
E-mail address: m_ghaedi@mail.yu.ac.ir; m_ghaedi@yahoo.com (M. Ghaedi)

Abstract

In the present work, the usefulness of ultrasonic power as dispersion and mixing tool to accelerate the adsorption of Safranin O (SO), Methylene blue (MB), Pb^{2+} ions and Cr^{3+} ions onto novel composite of Fe_3O_4-NPs-AC as adsorbent was investigated. This new material extensively were characterized and analyzed by different techniques such as XRD, FESEM, Raman spectroscopy and FT-IR. The Central Composite Design (CCD) based on designed runs reveal that adsorbent mass, sonication time, MB concentration, SO concentration, Pb^{2+} ions and Cr^{3+} ions concentration and some of their interactions have significant contribution on the target compounds removal percentages. The combination of response surface methodology and Design-Expert software used to qualify and estimates the influence and magnitude of each term contribution on response. The optimization over following investigated interval of effective variables, adsorbent mass (0.01-0.03 g), sonication time (2-6 min), initial dyes concentration (5-25 mg L^{-1}), initial metal ions concentration (20-60 mg L^{-1}) reveal that fixing the experimental variables at 0.025 g of Mn-Fe_3O_4-NPs-AC, 3 min sonication time, 20 mg L^{-1} of MB, 10 mg L^{-1} of SO, 38 mg L^{-1} of Pb^{2+} ions and 42 mg L^{-1} of Cr^{3+} ions at room temperature lead to achievement of best characteristics performance. Conduction of 32 experiments according to limitation of CCD and their subsequent analysis of variance (ANOVA) gives useful information about significant and also approximate contribution of each term (main and interaction of variables) in empirical equation on expected response. The results indicate that the R^2 values are more than 0.988 and adjusted R^2 are in a reasonable agreement with R^2. Under the optimal conditions, the MB, SO, Pb^{2+} ions and Cr^{3+} ions removal efficiency reached 99.54%, 98.87%, 80.25% and 99.54% after 3 min, while their equilibrium data with high performance can be represented with Langmuir isotherm and a pseudo second-order kinetic model. The maximum adsorption capacity in single component system, 229.4 mg g^{-1} for MB, 159.7 mg g^{-1} for SO, 139.5 mg g^{-1} for Pb^{2+} ions and 267.4 mg g^{-1} for Cr^{3+} ions support high efficiency of Mn-Fe_3O_4-NPs-AC as new adsorbent.

Keywords: Adsorption, Dyes, Heavy metals, Mn-Fe_3O_4-NPs-AC, Nanoparticles, Response surface methodology, Ultrasound-assisted removal.

.

1. Introduction

Environmental pollution as greatest ecosystem problem seriously damage the human health and other organism life forms.[1] Main attention and hazards are devoted to the presence of dyes and heavy metals that subsequently generate very serious environmental problems. These expected limitations and hazards is concerned to their toxic effects, non-biodegradability, accumulation in living tissues which possible their simple arrival to the human and animal bodies through food consumption.[2-4]

Lead source including battery, mining, lead smelting, metal plating, paper and pulp, metallurgical finishing and metal processing into the environment.[5] Cr^{3+} ions act as useful and essential element for humans, while its high content is toxic.[6, 7] Chromium is utilized in industries like electroplating, leather tanning, metal finishing, and nuclear power plant and textile and chromate preparation manufacturers. Chromium is considerably carcinogenic and causes problems such as chromosomal abnormality and bioaccumulation into flora and fauna.[8, 9] Dye present in wastewater come from textile, leather, paper, and plastics consume, while methylene blue (MB; Fig. 1, thiazine cationic dye) has extensive application in industry, biology and chemistry.[10, 11]

Safranin-O (SO, reddish brown powder, Fig. 1) also is a cationic (azine) dye belong to synthetic dyes[12] with high dissolubility in water and extensively applied in food products for flavoring and coloring candies and cookies in addition to tannin, cotton, fibers, wool, silk, leather and paper coloring and treatment.[13]

All above mention hazards related to dyes and understudy metal ions encourage the researchers to design and develop novel method for their efficient and quantitative removal by a simple, low cost and fast procedure. A method that applicable for their simultaneous efficient removal in short time with low consumption of reagents is highly recommended.

These wide application make emphasis on researchers to efficiently conduct process for removal of SO and MB. The more common treatment techniques that have been used to reduce the heavy-metal and dyes content in wastewaters to permissible concentrations include adsorption, biosorption,[14-16] chemical precipitation,[17] electrokinetic coagulation,[18] reverse osmosis,[19] ion exchange,[20] filtration and membrane,[21] ozonation,[22] fungal decolorization,[23] and adsorption [24-32] processes.

Among them, adsorption based on their unique offer-mentioned properties has talent to be as best promising technologies for environment cleaning from heavy metals and dyes.[33, 34] Combination of unique properties of adsorption with distinct ability and prominent properties of nano-scale materials cause achievement of simultaneous adsorption and removal of dyes and pollutants. These protocols can be accomplished with application of mathematical models to relevance and evaluate the statistical significance of factors and their interaction[29, 35-37] that permits development of low cost and short time clean up systems. Multivariate designs composed of different stages such as responses analysis (qualitative or quantitative) and lateral estimation and express of its dependency to factors (sole and interaction) using at least experiments.

This procedure is superior to one way classification and optimization in term of requirement of large number of experiments and serious time reduction, while impossible to exactly give idea about variables interactions.[38] These problems simply can be resolved with at least possible number of experiments namely response surface methodology (RSM) in different branches. [36]

The purpose of this study was to investigate the adsorption characteristics of dyes and heavy metal ions by Mn doped Fe_3O_4-NPs loaded on AC. The effects of experimental parameters such as adsorbent mass, sonication time and initial concentration of target compounds on their adsorption were analyzed using RSM. The isotherm and kinetic parameters were also evaluated using the adsorption measurements. The maximum capacity (Q_{max}) of adsorbent was comparable to other adsorbents.

2. Experimental

2.1. Instruments and reagents

Ammonium iron (III) sulfate (NH_4 Fe $(SO_4)_2.12H_2O$), iron (II) sulfate ($FeSO_4.\ 7H_2O$), Manganese sulfate ($MnSO_4.\ 2H_2O$) were purchased from Sigma company (St. Loius, MO, USA). Sulfuric acid ($ZnSO_4.\ 2H_2O$), Lead (II) nitrate ($Pb(NO_3)_2.\ 2H_2O$), Chromium (III) nitrate (Cr $(NO_3)_3.\ 9H_2O$), HCl, sodium hydroxide (NaOH), MB and SO (Merck, Dermasdat, Germany) used as received and their solutions were prepared by dissolving their appropriate amount in double distilled water. In all stages, the pH was adjusted using pH/Ion meter model-686 (Metrohm, Switzerland, Swiss). Absorbance spectra of MB, SO (Fig. 1) were taken in a wide range of wavelength (λ) from 400 to 750 nm, using UV–Visible spectrophotometer model V-530

(Jasco, Japan) with a fixed slit width of 2 nm and scan speed of 1000 nm/min. Heavy metal ions analysis was carried out by using flame atomic absorption spectrophotometer (FAAS) Varian model AA 240 (USA). The Fe_3O_4 nanoparticles were characterized by FESEM (Hitachi. S4160, Japan), XRD (PW 1800, Philips, Germany) and A Fourier transform infrared (FT-IR) spectrum was recorded using a Perkin Elmer-Spectrum-RX-IFT-IR spectrometer in the range of 400–4000 cm^{-1}. Raman spectra were recorded in the backscattering geometry in the range 200–2000 cm^{-1} using a Handheld Raman Analyzer Raman spectrometer (model-™FIRSTGUARD, RIGAKU). Particle size distribution of the samples was determined using a particle size Qudix, ScatterO Scope (I) system (Korea) at 25 ˚C. An ultrasonic bath with heating system (Tecno-GAZ SPA Ultra Sonic System, Parma, Italy) at 40 kHz of frequency and 130 W of power was used for the ultrasound-assisted adsorption procedure. A HERMLE bench centrifuge (2206A, Germany) was used to accelerate the phase separation.

2.2. Synthesis of Mn doped Fe_3O_4-NPs loaded on AC

The reaction solution for synthesis of Mn doped Fe_3O_4 nanoparticles was prepared as follows: first 10 g of ammonium iron (III) sulfate, 5.0 g iron (II) sulfate solution and 5.0 g manganese sulfate were dissolved (by 6 mL of concentrated sulfuric acid at pH= 2.4) and mixed thoroughly in 20 mL deionized water. Then, 130 mL distilled water and 20 g activated carbon (AC) were added to above solution and 140 mL of 1.5 mol L^{-1} sodium hydroxide was added drop-by-drop during 70 minutes along with strong stirring at room temperature in an Erlenmeyer flask. After 70 minutes, again 100 mL of 3 mol L^{-1} sodium hydroxide solution was added to the mixed reaction solution drop-by-drop during 40 minutes at room temperature. The prepared reaction solution was stirred strongly for 27 hours at room temperature. The Mn doped Fe_3O_4-NPs loaded on AC were filtered and washed several times by distilled water and dried at 35 ºC for 15 hours and finally characterized and used as an absorbent for adsorptions experiments.

2.3. USA- adsorption method

The simultaneous removal of dyes and under study metal ions was examined using ultrasonic power combined Mn-Fe_3O_4-NPs-AC. The adsorption experiment was assisted by the ultrasonic waves and the influence of variables i.e. adsorbent mass, sonication time, initial SO, MB, Pb^{2+} and Cr^{3+} concentrations in quaternary system removal were examined and optimized values were

found to be 0.025 g, 3 min, 20, 10, 38 and 42 mg L^{-1}, respectively, at the desired temperature (25 ºC). At the end of the adsorption experiments, the sample was immediately centrifuged and the magnitude of non-adsorbed target compounds was analyzed via UV–Vis spectrophotometer and/or flame atomic absorption spectrometry, respectively.

2.4. Kinetics and adsorption isotherms

For this purpose 0.01, 0.015 and 0.02 g of adsorbent was contacted with 50 mL of analytes solution at optimum conditions viz. ultrasonic at 25 ºC for different time intervals at pH 5.0. The samples were filtered and analytes content were determined and experimental data at various times were fitted to different models such as pseudo first, second-order, intraparticle diffusion and elovich models. The experiments were also performed in the initial dyes and ions concentrations range of 5–50 mg L^{-1} to obtain adsorption isotherms. A series of solutions with different concentrations of understudy compounds were prepared by proper dilution of their stock solution and 50 mL of each solution was mixed with 0.01, 0.015 and 0.02 g of Mn-Fe_3O_4-NPs-AC and agitated for 3 min in ultrasonic at 25 ºC at pH 5.0. The samples were filtered and the non-removed content of each species were quantified according to calibration curve achieved at similar conditions. Finally, their equilibrium data were fitted to conventional isotherm models like Langmuir, Freundlich, Temkin and Dubinin-radushkevich and the corresponding parameters of each model were calculated from the respective graphs.

2.5. Measurements of dye uptake

The dye concentrations were determined according to calibration plots achieve at the same conditions. The dyes and ions removal percentage (R %) was calculated using the following equation:

$$\text{Percent removal.}(\%) = \frac{C_0 - C_t}{C_0} \times 100\% \quad (1)$$

Where C_0 (mg L^{-1}) and C_t (mg L^{-1}) are the dye concentration at initial and after time t respectively and the equilibrium adsorption capacity of dyes was calculated according to Eq. (2):

$$q_e = \frac{(C_0 - C_e)V}{W} \quad (2)$$

where C_0 (mg L^{-1}) and C_e (mg L^{-1}) are the initial and equilibrium dye concentrations in solution, respectively, V (L) is the volume of the solution and W (g) is the mass of the adsorbent.

2.6. Response surface methodology (RSM)

Optimum conditions for the efficient and quantitative adsorption of target compounds onto Mn-Fe_3O_4-NPs-AC were determined by means of central composite design (CCD) under RSM as useful simultaneous optimization technique.[39] There are three main steps involved in this process: experimental design, modeling, and optimization. This model provides relatively few combinations of variables for the determination of complex response function.[40]

A six-factor (A, B, C, D, E and F) and five-levels (-α, -1, 0, +1 and +α) CCD with minimum number of experiments, while adsorbent mass (A. g), sonication time (B, min), MB concentration (C, mg L^{-1}), SO concentration (D, mg L^{-1}), Pb^{2+} ions concentration (E, mg L^{-1}) and Cr^{3+} ions concentration (F, mg L^{-1}) are used in optimization section. The dependent variable (response variable) was the species removal percentages and each variable was coded five levels (-α, low, central, high and +α; Table 1).

The minimum and maximum levels (Table 1) given to each factor were chosen based on preliminary experiments. Each experiment was performed in double and the average values were taken as the response (R %). Fitting and analysis of experimental data approximately follow second-order polynomial model with acceptable estimated regression coefficients. The generalized second order polynomial model proposed for the response surface analysis was given as follows:

$$y = \beta_0 + \sum_{i=1}^{k} \beta_i x_i + \sum_{i=1}^{k} \sum_{j=1}^{k} \beta_{ij} x_i x_j + \sum_{i=1}^{k} \beta_{ii} x_i^2 + \varepsilon \quad (3)$$

where y is the predicted response; X_i and X_j are the coded values of independent variables; and β_0, β_i, β_{ii} and β_{ij} are the regression coefficients for intercept, linear, quadratic and interaction

terms, respectively. ε represents the random error and k is the number of factors. In this experiment, k=6. Data were processed for Eq. (3). Design-Expert program including ANOVA (Analysis of Variance) based on well-known F and P-value give very constructive and useful information about main effect and interactions between variables and also their contribution on the response.

The goodness of fit of the quadratic model was expressed by the coefficient of determination R^2, and its statistical significance was checked by the Fisher's F-test in the same program. In the present study a total of 32 runs were carried out to estimate the coefficients and lateral generated mathematical model was validated by conducting experiments at optimal values of variables predicted by response optimization.

The optimum values of selected variables were obtained by solving the regression equation and by evaluating the response surface plots. The response surface plots are used for analysis of different interaction between independent variables while keeping the value of the six variables as constant. Such three dimensional plots give accurate geometrical representation and provide useful information about the behavior of the system.

3. Results and discussion

3.1. Characterization of Mn doped Fe_3O_4 nanoparticles

FE-SEM image was used to determine the morphology and the particle size of the prepared Mn doped Fe_3O_4-NPs (Fig. 2a) that suggest essentially spherical shaped particles with the approximately size of 40 nm. The particles are almost uniform in the shape and the size.

The particle size frequency of the sample was measured by using particle size analysis technique and shown in Fig. 2b. According to the obtained results the average size of particles was 124 nm.

Fig. 3a shows the XRD pattern of the prepared Fe_3O_4 nanoparticles. The six peaks observed in diffractogram at 2θ= 30.1, 35.3, 43.1, 56.9, 62.10, and 70.5° are related to (220), (311), (400), (511), (440), and (620) lattice planes of magnetite (Fe_3O_4) and/or maghemite (γ-Fe_2O_3), respectively (JCPDS No.19-0652 and 04-0755), Because XRD patterns of maghemite (γ-Fe_2O_3) and magnetite (Fe_3O_4) are practically identical,[41] X-ray diffraction alone cannot be used to distinguish between the two phases. Therefore, we employed Raman spectrophotometry technique to distinguish between these two phases. In the XRD pattern, no characteristic peaks of impurity phases such as $Fe(OH)_2$ and/or $Fe(OH)_3$ were detected.

Raman spectroscopy can effectively distinguish between maghemite and magnetite nanoparticles. Raman spectrum of the prepared sample was shown in Figure 3b. Raman features of Fe_3O_4 are sample specific, depending on non-stoichiometry, cation distribution, defects, and also on the experimental conditions. Nevertheless, the Raman spectra of magnetite are distinct from those obtained from maghemite.[42] Mandal *et al* [43] reported the presence of distinct peaks at 283 cm^{-1},490 and 668 cm^{-1} for undoped Fe_3O_4 nanoparticles, which correspond to the E_g, T_{2g} and A_g modes, respectively. Besides, in the published reports, in the Raman spectra the characteristic peaks of the Fe_3O_4 appeared at 668, 540, 450-500, 350 and 306 cm^{-1},[42] whereas γ-Fe_2O_3 shows broad bands around 700 and 500 cm^{-1} and α-Fe_2O_3 shows the resonant peaks at 225, 245, 291, 410, 611 and 1318 cm^{-1}. [42-45]

In our study, the Raman spectrum of the prepared sample (Fig. 3b) shows three peaks at 438, 455, and 479 cm^{-1}. The results were compared with the different published results and assigned as T_2g mode of symmetry of Fe_3O_4, while the peaks at 500, and 700 cm^{-1} belonging to γ-Fe_2O_3 as well as the peaks related to α-Fe_2O_3 were not observed in our results.[42-45] Therefore, the Raman analysis confirmed that the chemical composition of the prepared sample in this experiment is Fe_3O_4. The rather weak peak at 1620 cm^{-1} is related to the $\delta(H_2O)$ mode.

The FT-IR spectrum of the prepared Mn doped Fe_3O_4-NPs (Fig. 3c) indicate strong and broad absorption bands at 530 cm^{-1} and 431 cm^{-1} are assigned to Fe-O stretching and bending vibration modes of Fe_3O_4, respectively.[46] The strong and broad absorption peaks about 3200-3375 cm^{-1} and 1600 cm^{-1} are attributed to normal polymeric O-H stretching vibration and H-O-H bending vibration of H_2O adsorbed in the Fe_3O_4 lattice,[46, 47] respectively.

3.2. Effect of pH

Solution pH is serious effective parameters in controlling adsorption seems with important influences on the solubility and chemistry, charge and abundance of metal ions, surface charge of adsorbent, dissociation and/or protonation of analytes and adsorbent functional groups.[48] Typical results assigned to effect of pH on the removal efficiency (%) of Pb^{2+} ions illustrated in Fig. 4a. Owing to the fact in pH less than 3 due to formation of positive charge simultaneously on adsorbent and metal ions and in pH higher than 7 due to formation of hydroxide complex or probable precipitation as hydroxide form an expectable reduce in removal efficiency was observed. Increasing pH from 2 to 5 for Pb^{2+} ions cause removal percentage raising from 40-60%

to 97.08% and the adsorption capacity increased. Result also reveal that for Cr^{3+} ions removal percentage was highly pH-dependent and increases with increasing solution pH. At pH < 4.0, the Cr^{3+} ions adsorption was increased slowly and reaches its maximum value at pH 4.0-5.5 and subsequently reach plateau. At low pH, competition among proton and Cr^{3+} ions for the same binding sites of adsorbent lead to reduce in removal percentage.[26] Rising the pH, lead to enhance in the number of negative charge sites of adsorbent that facilitate the adsorption of cationic Cr^{3+} ions. Fig. 4a shows the adsorption process as pH function and reveal that adsorption favored at higher pH and suggest presence of more negative charged sites available on adsorbent which accelerate adsorption through electrostatic attraction and/or complexation, while the percentage of hydrolyzed Cr^{3+} ions increased.[49] The neutral pH was found to be optimum for the MB and SO adsorption. At lower pH, adsorption of high content of proton on adsorbent surface leads to the generation of net positive charge, which increases electrostatic repulsive force and thus decreases the adsorption of MB and SO molecules. At 5.0-7.0 pH which is the working pH in this research maximum removal percentage was seen. In compromise to achieve maximum removal percentage for all species pH was set at approximate 5.0.

3.3. Statistical analysis

The CCD and corresponding results of RSM experiments in the following interval of variable: A (0.01-0.03 g), B (2-6 min), C (5-25 mg L^{-1}), D (5-25 mg L^{-1}), E (20-60 mg L^{-1}) and F (20–60 mg L^{-1}) on removal percentages of compounds are given in Table 1. The design suggested the second-order polynomial model for the responses selected on the basis of the sequential model sum of squares where the additional terms were significant and the models were not aliased. The ‘‘Predicted R-Squared’’ was close to ‘‘Adjusted R-Squared’’. The quality of model was justified based on the R^2 and standard deviation values (Table S1). The ratio for the % R_{MB}, % R_{SO}, % $R_{Pb}{}^{2+}$ and %$R_{Cr}{}^{3+}$ responses were 17.65, 34.24, 16.35 and 22.21, respectively. Their value greater than 4 confirms the adequacy of model for representation of experimental data.

The removal percentage results in second-order response surface by ANOVA (Tables 2 and 3) demonstrate that all the models were significant at the 5% confidence level (*P*-values less than 0.05). The R^2 value close to unity and lower standard deviation strongly support high performance of method in term of larger accuracy and repeatability of model for prediction of real behavior of adsorption system. The values of coefficient of determinations (R^2= 0.989,

0.997, 0.991 and 0.995) obtained in the present study for $\%R_{MB}$, $\%R_{SO}$, $\%R_{Pb}^{2+}$ ions and $\%R_{Cr}^{3+}$ responses were higher than 0.80 as minimum acceptable value.

A high R^2 value close to 1 demonstrates good agreement between the calculated and observed results within the range of experiment and also has desirable and reasonable trend with adjusted R^2.[50] The data were analyzed to examine the correlation between the actual or experimental and predicted responses for dyes and ions (Fig. 4b). The data points were well distributed close to a straight line with the R^2 values of 0.989, 0.997, 0.991 and 0.995 for $\%R_{MB}$, $\%R_{SO}$, $\%R_{Pb}^{2+}$ ions and $\%R_{Cr}^{3+}$, respectively (excellent relation among experimental and predicted values).[51]

Tables 2 and 3 gives ANOVA results for respective responses and based on well-known phenomena the highly significant regression model is justified by higher Fischer's '*F* statistics' values with '*P*' value (probability) as low as possible.[52]

The variables denoted in ANOVA (Table 2 and 3) were the main effects, the interaction effects, and the error terms. F and p-values were used to represent the importance of these variables in the quadratic model. In addition, the sum of squares (SS), degrees of freedom (DF), and mean squares (MS) were calculated. The F-value was obtained by dividing MS by DF, whereas the MS value obtained by dividing SS by DF.[53]

The Model F-value of 12.92, 52.78, 16.51 and 27.24 for removal of MB, SO, Pb^{2+} and Cr^{3+} ions, respectively, implies the goodness and usefulness of presented model. Moreover, the quality of fitness models was assessed by a lack-of-fit test ($p > 0.05$ for all responses); this test determines model accuracy to predict variation. The high reliability and precision of the response data were confirmed by values of coefficient of variation (CV %) that varied between 0.610-3.221. Adequate precision is a statistical index that indicates signal to noise ratio; values higher than 4 are acceptable. For all responses studied, this indicator is greater than 4 (Table S1).

The 'F' and 'P' values (Tables 2 and 3) using standardized main effect Pareto charts (P = 95%) and two factor interaction Pareto charts (P = 95%) (Fig. S1) reveal that the factors of A, B and the quadratic effect of A^2 are the most effective factors and thus the empirical equation are as follows:

$$y_{MB} = 126.8 + 502.4A + 1.6052\,B - 0.434\,C + 16.9\,AC + 9.29\,AF - 0.0225\,CD + 0.0202\,CF + 0.037\,DE - 305\,A^2 + 0.0033\,E^2 + 0.004\,F^2 \quad (4)$$

$$y_{SO} = 99.26 + 5666\,A + 0.455\,B - 6.8\,D + 117.1\,AC + 193.21AD - 0.16\,BE + 0.22\,BF - 0.111\,CD - 0.064\,CE + 0.0583\,CF + 0.132\,DE - 226549.6\,A^2 \quad (5)$$

$$y_{Pb^{2+}} = -39.294 + 3802.2\,A - 13.756\,B + 1.0048\,C + 5.4\,D + 2.62\,E - 0.0185\,EF - 0.017\,E^2 \quad (6)$$

$$y_{Cr^{3+}} = -49.3 + 2158.6\,A + 7.84\,B + 1.93\,E + 0.832\,F - 1122\,AB + 72.7\,AE + 89\,AF + 0.89\,BD + 0.51\,BE - 0.25\,DE - 90812\,A^2 - 1.6\,B^2 - 0.03\,E^2 - 0.04\,F^2 \quad (7)$$

3.4. Effect of variables and response surface 3D plots

Figs. 5 and 6 demonstrate the fitted response surface and contour plots of removal (%) across important variables. The bents nature of curves is good indication of interaction between the parameters.

According to Figs. 5 (a, b) and 6 (a), the response surface plots show the relation among initial analytes concentration and amount of adsorbent, while the initial pH and sonication time were kept constant at 5 and 4 min (the central levels), respectively. The increase in analytes removal efficiency with rising adsorbent mass (Figs. 5 and 6) is emerged from the higher available surface area of adsorbent.

It was evident that the adsorption efficiency considerably increased with an increase in adsorbent dose due to its high effective surface area for adsorption. At lower amount of adsorbent, the removal percentage significantly decreased because of high ratio of analytes molecules to vacant site of adsorbent.

Figs. 5(c) and 6(c) shows the interaction of adsorbent mass with sonication time and their relation with removal percentage. The maximum adsorption of analytes achieved in high sonication time that confirm strong association of ultrasound in mass transfer. The results show that the initial adsorption rate is very rapid because of high available surface area and vacant site of adsorbent that accelerated by enhance in mass transfer by ultrasonic power.

It may be seen from the figures (Figs. 5c and 6c) that the increase in amount of adsorbent dose leads to significant decrease in sonication time. On the other hand, percentage dye removal was increased with the amount of adsorbent for a particular sonication time.

Fig. 6(b) clearly indicates that as the adsorbent mass and sonication time increases, the adsorption efficiency improves. It could be explained by the fact that the more amounts of Mn-Fe_3O_4-NPs-AC cause an increase in the adsorbent surface as well as active surface. The active surfaces prepare some spaces for capturing Cr^{3+} ions molecules and increasing these spaces makes the Cr^{3+} get out faster.

3.5. Optimization of dyes and ions adsorption

In the numerical optimization, a minimum and a maximum level must be provided for each parameter. A multiple response method or optimization of any combination of six objectives namely A, B, C, D, E and F was applied. Fig. 7 and Table S2 results illustrate the ranges of parameters obtained from the model (their exact value shown by the circles). The bottom lines show the recovery of dyes and ions at horizontal range. By optimizing the process parameters to obtain maximum removal of MB, SO, Pb^{2+} and Cr^{3+} ions under these conditions: adsorbent mass = 0.025 g, sonication time = 3 min, MB concentration = 20 mg L^{-1}, SO concentration = 10 mg L^{-1}, Pb^{2+} ions concentration = 38 mg L^{-1} and Cr^{3+} ions concentration = 42 mg L^{-1}, maximum removal of 99.54% for MB, 98.88% for SO, 80.25% for Pb^{2+} and 99.54% for Cr^{3+} was achieved.

3.6. Kinetics of dyes and ions adsorption onto Mn-Fe_3O_4-NPs-AC

In the present study, the appropriate kinetic model was investigated for explaining the nature of adsorption process. To investigate the mechanism of adsorption and rate controlling steps such as chemical reaction and diffusion control, conventional kinetic models including pseudo-first-order, pseudo-second-order, intraparticle diffusion and Elovich were used.

The pseudo-first-order kinetic model known as the Lagergren [54] equation is given as:

$$\log(q_e - q_t) = \log q_e - (\frac{k_1}{2.303})t \quad (8)$$

where q_e and q_t refer to the amount of analytes (mg g^{-1}) at equilibrium and at any time, respectively and k_1 is the equilibrium rate constant of pseudo-first-order adsorption (min^{-1}). The plot of log (q_e-q_t) vs. t should give a linear relationship which the value of k_1 was determined from the slope of the plot (Table 4).

The results show (Table 4) that the theoretical q_e (calc) value does not agree to the experimental q_e (exp) values at all concentrations studied with poor correlation coefficient. So, further the experimental data were fitted with second order Lagergren model.

The pseudo-second-order rate equation developed by Ho and McKay assumes that the adsorption capacity of adsorbent is directly proportional to the number of active sites on its surface.[55] The pseudo-second-order rate expression is given as:

$$\frac{t}{q_t} = \frac{1}{k_2 q_e^{\,2}} + \frac{t}{q_e} \qquad (9)$$

where k_2 (g mg^{-1} min^{-1}) is the equilibrium rate constant for the pseudo-second-order adsorption and can be obtained from the plot of t/q_t against t (Table 4).

The adsorbate species are most probably transported from the bulk of the solution into the solid phase with an intraparticle diffusion process with general applicability as rate-limiting step in many adsorption processes which can be explained by following well known equation:[10]

$$q_t = K_{dif} t^{1/2} + C \qquad (10)$$

where C is the intercept and K_{dif} is the intra-particle diffusion rate constant. The values of K_{dif} (g mg^{-1} $min^{-1/2}$) and C and the corresponding linear regression correlation coefficient R^2 are given in Table 4.

The applicability of intraparticle diffusion model imply that adsorption process of the dyes was a complex process involving both boundary layer and intraparticle diffusion.

The constant C was found to increase from 17.960 to 170.48 with increase in analytes amount from 10 to 42 mg L^{-1} at 0.01–0.02 g of Mn-Fe_3O_4-NPs-AC. A larger C value indicates a greater effect of the boundary layer.

This change in C value is belong to increase in thickness of the boundary layer and decrease the chance of the external mass transfer and subsequently prominent increase in the amount of internal mass transfer. The high value of R^2 shows suitability of this model to explain the experimental data. This may confirm that the rate-limiting step is the intraparticle diffusion process.

The Elovich equation is useful in describing adsorption on highly heterogeneous adsorbent. The Elovich [56] model is given by:

$$q_t = \frac{1}{\beta}\ln(\alpha\beta) + \frac{1}{\beta}\ln t \quad (11)$$

The q_t is a linear function of ln (t) if the Elovich would apply where β and α would be obtained from the slope and intercept of the plot of the Elovich equation, respectively.

The Elovich constants obtained from the slope and the intercept of the straight line are reported in Table 4. The low correlation coefficient of this model shows the unsuitability of it for evaluation of the adsorption process.

The kinetic constants and correlation coefficients of the pseudo-first-order, pseudo-second-order, intraparticle diffusion and elovich are presented in Table 4. At all concentrations and adsorbent amount, the calculated q_e values were mainly closer to the experimental data and the R^2 values for pseudo-second-order kinetic model were larger than that of pseudo-first-order model. These two simultaneous trends reveal the pseudo-second order model is more suitable for describing the adsorption behavior of dyes and ions onto Mn-Fe_3O_4-NPs-AC. Generally, the intraparticle diffusion model possesses two parts that are attributed to phenomena such as initial surface adsorption and subsequent intraparticle diffusion. The R^2 value (Table 4) for this model was near from the unity, which shows that the intraparticle diffusion model is applicable.

3.7. Adsorption isotherms

Langmuir isotherm[57] is based on adsorption on homogeneous sites as monolayer with uniform strategies with no transmigration of adsorbate in the plane of the surface. The linear form of Langmuir isotherm equation is given as:

$$\frac{C_e}{q_e} = \frac{1}{Q_m k_L} + \frac{C_e}{Q_m} \quad (12)$$

where C_e is the equilibrium concentration of adsorbate (mg L^{-1}); q_e is the adsorption capacity (mg g^{-1}); k_L and Q_m are the Langmuir constants. The values of Langmuir constants k_L and Q_m were

calculated from the slope and intercept of the linear plot of C_e/q_e versus C_e.

The fitness of experimental data was evaluated at different levels of adsorbent dosage. The high correlation coefficient (0.993-0.999) at all adsorbent dosage and high maximum monolayer capacity (91.99-267.4 mg g^{-1} using 0.01-2.0 g adsorbent) show the applicability of Langmuir model for interpretation of the experimental data over the whole concentration ranges.

The essential feature of the Langmuir isotherm can be expressed in terms of dimensionless constant separation or equilibrium parameter (R_L), which is defined as:

$$R_L = \frac{1}{1 + K_L C_0} \quad (13)$$

where C_0 is the initial analyte concentration (mg L^{-1}) and b is the Langmuir constant. The value of R_L calculated from different initial concentrations is reported in Table 5. The value of R_L indicates the type of the isotherm to be either unfavorable ($R_L > 1$), linear ($R_L = 1$), favorable ($0 < R_L < 1$) or irreversible ($R_L = 0$).[58] The obtained R_L values for dyes and ions between 0.009 and 0.230 suggest favorable adsorption of target compounds on Mn-Fe_3O_4-NPs-AC.

The following linear Freundlich [59] equation was applied for fitting the experimental data.

$$\ln q_e = \ln K_F + \frac{1}{n} \ln C_e \quad (14)$$

where 1/n and K_F are the Freundlich adsorption isotherm constant and its respective correlation coefficient, respectively. The intercept and slope of linear plot of ln (q_e) versus ln (C_e) give the values of K_F and 1/n, respectively. The Freundlich constants were calculated and presented in Table 5.

The correlation coefficients (0.910–0.985) and higher error value of this model show that the Freundlich model has lower efficiency compared to the Langmuir model.

The heat of the adsorption and the adsorbent–adsorbate interaction were evaluated by using Temkin isotherm model:[60]

$$q_e = B_1 \ln K_T + B_1 \ln C_e \quad (15)$$

B_1 is the Temkin constant related to heat of the adsorption (J mol^{-1}), T is the absolute temperature (K), R is the universal gas constant (8.314 J mol^{-1} K^{-1}), K_T is the equilibrium binding constant (L mg^{-1}).

The correlation coefficients R^2 obtained from Temkin model were comparable to that obtained for Langmuir and Freundlich equations, which explain the applicability of Temkin model to the adsorption of dyes and ions onto adsorbent.

In order to calculate the mean free energy value of sorption, Dubinin–Radushkevich (D-R) isotherm has also been applied for the sorption of dyes and ions onto Mn-Fe_3O_4-NPs-AC. The D-R equation can be defined by the following equation:[61]

$$\ln q_e = \ln Q_S - B\varepsilon^2 \quad (16)$$

where B is the constant related to sorption energy (mol^2 J^{-2}), Q_S is the D–R monolayer capacity (mol g^{-1}), q_e is the amount of dye and ion sorption per unit weight of Mn-Fe_3O_4-NPs-AC (mg g^{-1}), ε is the Polanyi potential which can be obtained as follows:

$$\varepsilon = RT \ln\left(1+\frac{1}{C_e}\right) \quad (17)$$

where C_e is the equilibrium concentration of dyes and ions (mol L^{-1}), R gas constant and T the temperature (K). By plotting ln q_e versus ε^2, it is possible to determine the value of B from the slope and the value of Q_S from the intercept, which is ln Q_S.

The lower R^2 values (0.845–0.981) over the whole adsorbent dosage show unsuitability of D–R model for fitting the experimental data. In this case, the D–R equation represents the poorer fit of the experimental data than other isotherm equations.

The mean free energy E (kJ mol^{-1}) of sorption can be estimated by using B values as expressed in the following equation:[62]

$$E = \frac{1}{\sqrt{2B}} \quad (18)$$

The parameters obtained using above equations was summarized in Table 5 that suggest physical adsorption (mean free energy value is lower than 8 kJ mol^{-1}). Since E values are in the range of 2-7 kJ mol^{-1} at 0.01, 0.015 and 0.02 g of adsorbent, indicating that the adsorption process of dyes and ions were probably controlled as physically.

Langmuir isotherm fits the data better than Freundlich, Temkin and D-R isotherms which justified by its higher R^2 value (>0.993) that support more abundance for occurrence of understudy compound adsorption onto Mn-Fe_3O_4-NPs-AC takes place as monolayer sorption on a surface that is homogenous in sorption affinity.

The values of the Temkin constants and the correlation coefficient are lower than the Langmuir value. Therefore, the Temkin isotherm represents a worse fit of experimental data than the Freundlich isotherm but the Langmuir isotherm provides the best correlation for the experimental data.

As can be seen from Table 5, Mn-Fe_3O_4-NPs-AC sorbent used in this work has a relatively large sorption capacity in single component (229.4 mg g^{-1} for MB, 159.7 mg g^{-1} for SO, 139.5 mg g^{-1} for Pb^{2+} ions and 267.4 mg g^{-1} for Cr^{3+} ions) for the removal of dyes and ions from aqueous solution compared to some other sorbents reported in the literature in Table 6.

3.8. Comparison with other methods

The maximum sorption capacity Q_{max} (mg g^{-1}) is great criterion for judgment useful in scale-up considerations. Some studies have been conducted using various types of sorbents for MB, SO, Pb^{2+} and Cr^{3+} adsorption.[12, 26, 30, 63-80] Table 6 presents a comparison of the sonication time and sorption capacity of Mn-Fe_3O_4-NPs-AC with that reported for other sorbents. It can be seen from Table 6 that the adsorbent show a comparable sorption capacity with the respect to other sorbents, revealing that the Mn-Fe_3O_4-NPs-AC is suitable for the removal of dyes and ions from aqueous solutions since it has a relatively high sorption capacity.

4. Conclusion

The dyes and heavy metals is commonly released into the environment through wastewaters disposed from industries. Therefore, dyes and ions remediation prior to discharge is of great importance. Application of Mn-Fe_3O_4-NPs-AC could be as an effective adsorbent for removing the MB, SO, Pb^{2+} and Cr^{3+} from contaminated water resources. This study tried to synthesize and

characterize the new class of adsorbent examine their performance on MB, SO, Pb^{2+} and Cr^{3+} removal from aqueous solution using CCD under the RSM. Several parameters such as the adsorbent mass, sonication time, initial dyes concentration and initial ions concentration were investigated. The obtained results demonstrated the empirical models were satisfactorily ($p < 0.001$) fitted to the experimental data. All mathematical equations developed in this process demonstrated high determination coefficients (greater than 0.988) and insignificant lack of fit ($p > 0.05$). The optimum removal efficiency of MB, SO, Pb^{2+} and Cr^{3+} achieved by setting the experiment with adsorbent mass at 0.025 g, sonication time at 3 min, initial MB concentration at 20 mg L^{-1}, initial SO concentration at 10 mg L^{-1}, initial Pb^{2+} concentration at 38 mg L^{-1} and initial Cr^{3+} concentration of 42 mg L^{-1}. Results also prove that the RSM is a powerful tool for optimizing the operational conditions of dyes and ions removal efficiency using adsorbent. Conventional kinetic models were applied and it was seen that pseudo-second-order equation is suitable to fit the experimental data. Analysis of experimental equilibrium data to the Langmuir, Freundlich, and Temkin and Dubinin-Radushkevich isotherms shows that the Langmuir is the best model for the dyes and ions interpretation of equilibrium data. The obtained results demonstrated that adsorbent can promisingly be used as an efficient sorbent for dyes and heavy metals.

References

1. P. Xu, G. Zeng, D. Huang, S. Hu, C. Feng, C. Lai, M. Zhao, C. Huang, N. Li, Z. Wei and G. Xie, *Colloid. Surf. A: Phys. Eng. Aspec.,* 2013, **419**, 147-155.

2. T. K. Naiya, A. K. Bhattacharya and S. K. Das, *J. Colloid Interface Sci.,* 2009, **333**, 14-26.

3. J.-S. Lim, S.-M. Kim, S.-Y. Lee, E. A. Stach, J. N. Culver and M. T. Harris, *J. Colloid Interface Sci.,* 2010, **342**, 455-461.

4. Y. Pang, G. Zeng, L. Tang, Y. Zhang, Y. Liu, X. Lei, Z. Li, J. Zhang, Z. Liu and Y. Xiong, *Chem. Eng. J.*, 2011, **175**, 222-227.

5. A. Hosseini-Bandegharaei, M. Karimzadeh, M. Sarwghadi, A. Heydarbeigi, S. H. Hosseini, M. Nedaie and H. Shoghi, *Chem. Eng. Res. Des.*, 2014, **92**, 581-591.

6. M. N. Sahmoune, K. Louhab and A. Boukhiar, *Environ. Prog. Sustain. Energy*, 2011, **30**, 284-293.

7. G. Qin, M. J. McGuire, N. K. Blute, C. Seidel and L. Fong, *Environ. Sci. Technol.*, 2005, **39**, 6321-6327.

8. S. Sharma, B. Petrusevski and G. Amy, *J. Water. Sup: Res. .Technol.—AQUA*, 2008, **57**, 541-553.

9. S. Rengaraj, K.-H. Yeon and S.-H. Moon, *J. Hazard. Mater.*, 2001, **87**, 273-287.

10. M. Ghaedi, A. G. Nasab, S. Khodadoust, M. Rajabi and S. Azizian, *J. Ind. Eng. Chem.,* 2014, **20**, 2317-2324.

11. M. Ghaedi and S. N. Kokhdan, *Spectrochim. Acta, Part A.,* 2015, **136,** 141-148.

12. S. Kaur, S. Rani, R. Mahajan, M. Asif and V. K. Gupta, *J. Ind. Eng. Chem.,* 2015, **22**, 19-27.

13. V. Garg, R. Gupta, A. B. Yadav and R. Kumar, *Bioresour. Technol.*, 2003, **89**, 121-124.

14. R. Tabaraki, A. Nateghi and S. Ahmady-Asbchin, *Int. Biodeterior. Biodegrad.*, 2014, **93**, 145-152.

15. M. El Haddad, R. Slimani, R. Mamouni, M. R. Laamari, S. Rafqah and S. Lazar, *J. Taiwan Inst. Chem. Eng.*, 2013, **44**, 13-18.

16. A. Gundogdu, D. Ozdes, C. Duran, V. N. Bulut, M. Soylak and H. B. Senturk, *Chem. Eng. J.*, 2009, **153**, 62-69.

17. Y.-C. Lee, E. J. Kim, J.-W. Yang and H.-J. Shin, *J. Hazard. Mater.*, 2011, **192**, 62-70.

18. A. Wang, J. Qu, H. Liu and J. Ge, *Chemosphere*, 2004, **55**, 1189-1196.

19. H. Li, Y. Lin, Y. Luo, P. Yu and L. Hou, *J. Hazard. Mater.*, 2011, **192**, 490-499.

20. C.-H. Liu, J.-S. Wu, H.-C. Chiu, S.-Y. Suen and K. H. Chu, *Water Res.*, 2007, **41**, 1491-1500.

21. E. Alventosa-deLara, S. Barredo-Damas, M. Alcaina-Miranda and M. Iborra-Clar, *J. Hazard. Mater.*, 2012, **209**, 492-500.

22. G. Moussavi and M. Mahmoudi, *Chem. Eng. J.*, 2009, **152**, 1-7.

23. Y. Fu and T. Viraraghavan, *Bioresour. Technol.,* 2001, **79**, 251-262.

24. X. Ma, L. Li, L. Yang, C. Su, K. Wang, S. Yuan and J. Zhou, *J. Hazard. Mater.*, 2012, **209**, 467-477.

25. F. Ji, C. Li, B. Tang, J. Xu, G. Lu and P. Liu, *Chem. Eng. J.*, 2012, **209**, 325-333.

26. S. Yang, L. Li, Z. Pei, C. Li, J. Lv, J. Xie, B. Wen and S. Zhang, *Colloids Surf. A: Physicochem. Eng. Asp.,* 2014, **457**, 100-106.

27. V. K. Gupta and I. Ali, *J. Colloid Interface Sci.,* 2004, **271**, 321-328.

28. M. Ghaedi, A. Ghaedi, F. Abdi, M. Roosta, A. Vafaei and A. Asghari, *Ecotoxicol. Environ. Saf.*, 2013, **96**, 110-117.

29. M. Ghaedi, H. Mazaheri, S. Khodadoust, S. Hajati and M. K. Purkait, *Spectrochim. Acta, Part A.,* 2015, **135**, 479-490.

30. M. Ghaedi, M. Pakniat, Z. Mahmoudi, S. Hajati, R. Sahraei and A. Daneshfar, *Spectrochim. Acta, Part A.,* 2014, **123**, 402-409.

31. M. Ghaedi, P. Ghobadzadeh, S. N. Kokhdan and M. Soylak, *Arab. J. Sci. Eng.*, 2013, **38**, 1691-1699.

32. A. Sari and M. Soylak, *J. Serb. Chem. Soc.*, 2007, **72**, 485-494.

33. H. Gad, H. Omar, M. Khalil and M. Hassan, *J. Am. Sci.*, 2013, **9**, 95-106.

34. K. Rout, M. Mohapatra and S. Anand, *Dalton Trans.*, 2012, **41**, 3302-3312.

35. A. Asfaram, M. Ghaedi, S. Agarwal, I. Tyagi and V. Kumar Gupta, *RSC Adv.*, 2015, **5**, 18438-18450.

36. A. M. Ghaedi, M. Ghaedi, A. Vafaei, N. Iravani, M. Keshavarz, M. Rad, I. Tyagi, S. Agarwal and V. K. Gupta, *J. Mol. Liq.*, 2015, **206**, 195-206.

37. A. Asfaram, M. Ghaedi, S. Hajati, A. Goudarzi and A. A. Bazrafshan, *Spectrochim. Acta, Part A.,* 2015, **145**, 203-212.

38. M. Ghaedi, S. Hajati, A. Goudarzi and A. A. Bazrafshan, *Spectrochim. Acta, Part A.,* 2015, **145**, 203-212.

39. A. Kicsi, C. Cojocaru, M. Macoveanu and D. Bilba, *J. Environ. Prot. and Ecol.*, 2010, **11**, 614-622.

40. C. Toles, W. Marshall and M. Johns, *Carbon*, 1997, **35**, 1407-1414.

41. D. De Faria, S. Venâncio Silva and M. De Oliveira, *J. Raman Spectrosc.*, 1997, **28**, 873-878.

42. C. S. Kumar, *Raman spectroscopy for nanomaterials characterization*, Springer Science & Business Media, 2012.

43. M. Mandal, S. Kundu, S. K. Ghosh, S. Panigrahi, T. K. Sau, S. Yusuf and T. Pal, *J. Colloid Interface Sci.,* 2005, **286**, 187-194.

44. L. Slavov, M. Abrashev, T. Merodiiska, C. Gelev, R. Vandenberghe, I. Markova-Deneva and I. Nedkov, *J. Magn. Magn. Mater.*, 2010, **322**, 1904-1911.

45. K. Song, Y. Lee, M. R. Jo, K. M. Nam and Y.-M. Kang, *Nanotechnology*, 2012, **23**, 505401.

46. Y. Wang, L. Wang, T. Tian, X. Hu, C. Yang and Q. Xu, *Analyst*, 2012, **137**, 2400-2405.

47. A. Goudarzi, A. D. Namghi and C.-S. Ha, *RSC Adv.*, 2014, **4**, 59764-59771.

48. H. L. Vasconcelos, T. P. Camargo, N. S. Gonçalves, A. Neves, M. C. Laranjeira and V. T. Fávere, *React. Funct. Polym.,* 2008, **68**, 572-579.

49. V. C. G. D. Santos, A. d. P. A. Salvado, D. C. Dragunski, D. N. C. Peraro, C. R. T. Tarley and J. Caetano, *Quim. Nova*, 2012, **35**, 1606-1611.

50. M. Y. Noordin, V. C. Venkatesh, S. Sharif, S. Elting and A. Abdullah, *J. Mater. Process. Technol.,* 2004, **145**, 46-58.

51. S. Hajati, M. Ghaedi and H. Mazaheri, *Desalin. Water Treat.*, 2014, 1-15.

52. A. I. Khuri and S. Mukhopadhyay, *WIREs: Comp. Stats.,* 2010, **2**, 128-149.

53. P. Sudamalla, P. Saravanan and M. Matheswaran, *Environ. Res.*, 2012, **22**, 1-7.

54. S. Lagergren, *K. Svenska Vetenskapsakad. Handl.*, 1898, **24**, 1-39.

55. Y.-S. Ho and G. McKay, *Proc. Saf. Environ. Protect.*, 1998, **76**, 183-191.

56. M. Ghaedi, A. Ansari and R. Sahraei, *Spectrochim. Acta, Part A.,* 2013, **114**, 687-694.

57. I. Langmuir, *J. Am. Chem. Soc.*, 1916, **38**, 2221-2295.

58. A. A. Khan, R. Ahmad, A. Khan and P. K. Mondal, *Arab. J. Chem.*, 2013, **6**, 361-368.

59. H. Freundlich, *Z. Phys. Chem.*, 1906, **57**, 385-471.

60. M. Temkin and V. Pyzhev, *Acta Physicochim. U. R. S. S.,* 1940, **12**, 217-222.

61. M. Dubinin and L. Radushkevich, *Chem. Zentr.*, 1947, **1**, 875-889.

62. E. Akar, A. Altinişik and Y. Seki, *Ecol. Eng.*, 2013, **52**, 19-27.

63. M. Peydayesh and A. Rahbar-Kelishami, *J. Ind. Eng. Chem.,* 2015, **21**, 1014-1019.

64. M. Roosta, M. Ghaedi, A. Daneshfar, R. Sahraei and A. Asghari, *Ultrason. Sonochem.*, 2014, **21**, 242-252.

65. M. Ghaedi, S. Heidarpour, S. Nasiri Kokhdan, R. Sahraie, A. Daneshfar and B. Brazesh, *Powder Technol.*, 2012, **228**, 18-25.

66. L. Ai, C. Zhang and Z. Chen, *J. Hazard. Mater.*, 2011, **192**, 1515-1524.

67. L. Ai, C. Zhang, F. Liao, Y. Wang, M. Li, L. Meng and J. Jiang, *J. Hazard. Mater.*, 2011, **198**, 282-290.

68. M. Ghaedi, A. Ghaedi, M. Hossainpour, A. Ansari, M. Habibi and A. Asghari, *J. Ind. Eng. Chem.,* 2014, **20**, 1641-1649.

69. M. El Haddad, A. Regti, R. Slimani and S. Lazar, *J. Ind. Eng. Chem.,* 2014, **20**, 717-724.

70. S. Shariati, M. Faraji, Y. Yamini and A. A. Rajabi, *Desalination*, 2011, **270**, 160-165.

71. N. K. Rotte, S. Yerramala, J. Boniface and V. V. Srikanth, *Chem. Eng. J.*, 2014, **258**, 412-419.

72. N. Rahman and U. Haseen, *Ind. Eng. Chem. Res.,* 2014, **53**, 8198-8207.

73. A. M. Awwad and A. M. Farhan, *Am. J. Chem.*, 2012, **2**, 238-244.

74. Y.-H. Li, Q. Du, X. Peng, D. Wang, Z. Wang, Y. Xia and B. Wei, *Colloid. Surf. B: Biointerfaces*, 2011, **85**, 316-322.

75. M. Iqbal and R. Edyvean, *Mineral. Eng.*, 2004, **17**, 217-223.

76. M. Rashid and F. Khan, *J. Water Process Eng.,* 2014, **3**, 53-61.

77. M. Deravanesiyan, M. Beheshti and A. Malekpour, *J. Ind. Eng. Chem.,* 2015, **21**, 580-586.

78. A. Demirbaş, *Energy sources*, 2005, **27**, 1449-1455.

79. S. Tahir and R. Naseem, *Sep. Purif. Technol.*, 2007, **53**, 312-321.

80. N. S. Rajurkar, A. N. Gokarn and K. Dimya, *Clean - Soil, Air, Water,* 2011, **39**, 767-773.

Table. 1. Experimental factors and levels in the central composite design.

Factors	Levels				
	-α	Low (-1)	Central (0)	High (+1)	+α
A: Adsorbent mass (g)	0.01	0.015	0.02	0.025	0.03
B: Sonication time (min)	2	3	4	5	6
C: MB concentration (mg L^{-1})	5	10	15	20	25
D: SO concentration (mg L^{-1})	5	10	15	20	25
E: Pb^{2+} concentration (mg L^{-1})	20	30	40	50	60
F: Cr^{3+} concentration (mg L^{-1})	20	30	40	50	60

	Factors						R%			
Run	A	B	C	D	E	F	MB	SO	Pb^{2+}	Cr^{3+}
1	0.0150	3.00	10.00	10.00	30.00	30.00	98.43	87.72	66.00	94.41
2	0.0250	3.00	20.00	20.00	30.00	50.00	99.44	94.48	76.33	99.71
3	0.0150	5.00	10.00	20.00	50.00	50.00	97.54	83.82	53.20	84.22
4	0.0150	5.00	10.00	10.00	30.00	50.00	98.39	91.07	70.00	54.64
5	0.0250	5.00	10.00	10.00	50.00	50.00	98.50	90.68	61.40	98.86
6	0.0200	4.00	15.00	15.00	60.00	40.00	99.08	94.34	53.67	78.85
7	0.0250	3.00	20.00	10.00	50.00	50.00	99.33	93.82	67.40	97.29
8	0.0300	4.00	15.00	15.00	40.00	40.00	99.00	93.81	82.50	84.81
9	0.0200	4.00	15.00	15.00	40.00	40.00	98.12	94.64	72.00	99.91
10	0.0150	3.00	20.00	20.00	50.00	50.00	93.79	69.01	56.00	42.06
11	0.0200	4.00	15.00	15.00	20.00	40.00	98.03	90.39	80.00	98.13
12	0.0250	3.00	10.00	10.00	50.00	30.00	98.64	92.04	71.60	100.0
13	0.0100	4.00	15.00	15.00	40.00	40.00	89.36	47.88	66.75	96.56
14	0.0150	5.00	20.00	20.00	50.00	30.00	91.46	60.22	58.80	100.0
15	0.0250	5.00	10.00	20.00	30.00	50.00	96.98	93.27	75.33	89.36
16	0.0200	4.00	15.00	5.000	40.00	40.00	99.03	87.96	62.25	100.0
17	0.0200	4.00	15.00	15.00	40.00	60.00	98.99	93.21	78.00	95.36
18	0.0150	3.00	20.00	10.00	30.00	50.00	98.51	90.09	72.33	67.96
19	0.0200	2.00	15.00	15.00	40.00	40.00	97.32	95.64	69.75	100.0
20	0.0200	4.00	15.00	15.00	40.00	40.00	98.01	94.97	72.50	99.06
21	0.0200	4.00	15.00	25.00	40.00	40.00	97.50	87.02	48.75	99.73
22	0.0200	4.00	5.000	15.00	40.00	40.00	97.68	93.37	65.00	100.0
23	0.0200	4.00	15.00	15.00	40.00	40.00	97.70	92.92	70.75	100.0
24	0.0200	4.00	15.00	15.00	40.00	40.00	97.85	92.55	71.50	98.91
25	0.0250	3.00	10.00	20.00	30.00	30.00	97.00	91.53	72.67	97.36
26	0.0250	5.00	20.00	10.00	50.00	30.00	98.97	90.66	65.40	97.78
27	0.0250	5.00	20.00	20.00	30.00	30.00	98.58	93.87	72.33	100.0
28	0.0150	5.00	20.00	10.00	30.00	30.00	98.28	90.99	70.00	98.28
29	0.0150	3.00	10.00	20.00	50.00	30.00	98.83	91.24	58.80	62.15
30	0.0200	4.00	25.00	15.00	40.00	40.00	98.22	92.52	79.50	100.0
31	0.0200	6.00	15.00	15.00	40.00	40.00	99.19	92.86	68.00	94.11
32	0.0200	4.00	15.00	15.00	40.00	20.00	98.53	92.65	69.50	97.93

817 **Table. 2.** Analysis of variance (ANOVA) for removal dyes.

Response	R% MB					R% SO				
Source	SS[a]	Df[b]	MS[c]	F-value	P-value	SS	Df	MS	F-value	P-value
Model	123.7145	27	4.582019	12.91716	0.00145	3484.166	27	129.0432	52.78445	0.0007490
A	46.544	1	46.54400	131.2121	0.0003315	1054.908	1	1054.908	431.5046	< 0.0001
B	4.119943	1	4.119943	11.61452	0.02708	30.55118	1	30.55118	12.4968	0.02412
C	5.98407	1	5.984070	16.86967	0.01477	0.358729	1	0.358729	0.146736	0.7212
D	1.178884	1	1.178884	3.323389	0.1424	59.80826	1	59.80826	24.46426	0.007783
E	0.552322	1	0.552322	1.557049	0.2802	7.773372	1	7.773372	3.179657	0.1491
F	0.106585	1	0.106585	0.300473	0.6127	0.15794	1	0.15794	0.064604	0.8119
AB	0.181894	1	0.181894	0.512778	0.5135	6.964241	1	6.964241	2.848686	0.1667
AC	2.845478	1	2.845478	8.02168	0.04724	137.1348	1	137.1348	56.09428	0.001700
AD	0.889477	1	0.889477	2.507523	0.1885	124.4292	1	124.4292	50.89709	0.002041
AE	0.498979	1	0.498979	1.406669	0.3012	1.287371	1	1.287371	0.526592	0.5082
AF	3.455367	1	3.455367	9.741016	0.03549	0.340547	1	0.340547	0.139299	0.7279
BC	0.145271	1	0.145271	0.409534	0.5570	0.679027	1	0.679027	0.277752	0.6261
BD	0.112723	1	0.112723	0.317778	0.6030	17.68462	1	17.68462	7.233803	0.05468
BE	0.095114	1	0.095114	0.268136	0.6319	42.62158	1	42.62158	17.43413	0.01397
BF	1.227527	1	1.227527	3.460517	0.1364	25.30154	1	25.30154	10.34946	0.03237
CD	5.060833	1	5.060833	14.26698	0.01948	122.7055	1	122.7055	50.19203	0.002096
CE	2.70921	1	2.709210	7.637525	0.05066	155.7337	1	155.7337	63.70206	0.001336
CF	5.429844	1	5.429844	15.30726	0.01736	45.31502	1	45.31502	18.53587	0.01259
DE	17.77095	1	17.77095	50.09802	0.002103	232.0418	1	232.0418	94.91548	0.0006217
DF	1.140118	1	1.140118	3.214104	0.1475	0.404426	1	0.404426	0.165428	0.7050
EF	1.675489	1	1.675489	4.723367	0.09545	0.168039	1	0.168039	0.068736	0.8061
A^2	16.90845	1	16.90845	47.66656	0.002308	933.1771	1	933.1771	381.7112	< 0.0001
B^2	0.494916	1	0.494916	1.395215	0.3030	0.368976	1	0.368976	0.150928	0.7174
C^2	0.145903	1	0.145903	0.411316	0.5562	0.56262	1	0.56262	0.230137	0.6565
D^2	1.942125	1	1.942125	5.47504	0.07939	1.846224	1	1.846224	0.755188	0.4339
E^2	3.214546	1	3.214546	9.062118	0.03954	2.341387	1	2.341387	0.957732	0.3832
F^2	4.248818	1	4.248818	11.97783	0.02580	0.592826	1	0.592826	0.242492	0.6482
Residual	1.418894	4	0.354724			9.778881	4	2.44472		
Lack of Fit	0.966104	1	0.966104	6.401005	0.08542	3.759919	1	3.759919	1.874037	0.2645
Pure Error	0.45279	3	0.150930			6.018962	3	2.006321		
Cor Total	125.1334	31				3493.945	31			

818 [a] Sums of Squares
819 [b] Degrees of Freedom
820 [c] Mean Square

821 **Table. 3.** Analysis of variance (ANOVA) for removal ions.

Response	R% Pb^{2+}					R% Cr^{3+}				
Source	SS	Df	MS	F-value	P-value	SS	Df	MS	F-value	P-value
Model	2171.03	27	80.40852	16.51447	0.007185	5722.358	27	211.9392	27.2431	0.002737
A	124.0313	1	124.0313	25.47381	0.007246	69.0228	1	69.0228	8.872333	0.04079
B	57.78125	1	57.78125	11.86724	0.02618	61.73938	1	61.73938	7.936107	0.04797
C	78.125	1	78.125	16.04548	0.01605	0.000	1	0.000	0.000	1.0000
D	91.125	1	91.125	18.71545	0.01239	0.03753	1	0.03753	0.004824	0.9480
E	346.7222	1	346.7222	71.21056	0.001080	185.8963	1	185.8963	23.89549	0.008112
F	36.125	1	36.125	7.41943	0.05278	353.0382	1	353.0382	45.38026	0.002530
AB	9.61	1	9.61	1.973722	0.2328	503.4645	1	503.4645	64.71636	0.001296
AC	4.694444	1	4.694444	0.964155	0.3817	3.5072	1	3.5072	0.450823	0.5387
AD	10.95704	1	10.95704	2.25038	0.2080	27.92378	1	27.92378	3.58938	0.1311
AE	23.14815	1	23.14815	4.754217	0.09470	70.37897	1	70.37897	9.046658	0.03964
AF	0.017778	1	0.017778	0.003651	0.9547	316.8255	1	316.8255	40.7254	0.003094
BC	29.45333	1	29.45333	6.049189	0.06973	2.781847	1	2.781847	0.357584	0.5821
BD	2.56	1	2.56	0.525778	0.5085	317.1275	1	317.1275	40.76422	0.003088
BE	14.69444	1	14.69444	3.017977	0.1573	416.8157	1	416.8157	53.57835	0.001853
BF	34.00333	1	34.00333	6.983678	0.05742	1.091994	1	1.091994	0.140367	0.7269
CD	0.444444	1	0.444444	0.091281	0.7776	2.341538	1	2.341538	0.300986	0.6124
CE	1.21	1	1.21	0.248512	0.6443	33.37007	1	33.37007	4.289457	0.1071
CF	16.72454	1	16.72454	3.434921	0.1375	22.5629	1	22.5629	2.900281	0.1638
DE	0.668981	1	0.668981	0.137397	0.7297	820.5987	1	820.5987	105.4814	0.0005068
DF	0.001111	1	0.001111	0.000228	0.9887	0.355958	1	0.355958	0.045756	0.8411
EF	54.76	1	54.76	11.24673	0.02847	25.07777	1	25.07777	3.223548	0.1470
A^2	2.104395	1	2.104395	0.432205	0.5468	149.941	1	149.941	19.27373	0.01178
B^2	0.055153	1	0.055153	0.011327	0.9204	70.09208	1	70.09208	9.009781	0.03988
C^2	0.162729	1	0.162729	0.033422	0.8638	0.100438	1	0.100438	0.01291	0.9150
D^2	592.3135	1	592.3135	121.6506	0.0003841	0.017479	1	0.017479	0.002247	0.9645
E^2	82.0044	1	82.0044	16.84224	0.01481	231.2544	1	231.2544	29.72591	0.005499
F^2	0.073335	1	0.073335	0.015062	0.9082	415.504	1	415.504	53.40974	0.001864
Residual	19.47589	4	4.868972			31.11822	4	7.779555		
Lack of Fit	6.179014	1	6.179014	1.39409	0.3228	23.31108	1	23.31108	8.957605	0.05800
Pure Error	13.29688	3	4.432292			7.807137	3	2.602379		
Cor Total	2190.506	31				5753.476	31			

822

Table. 4. Kinetic parameters obtained from the simultaneous removal of dyes and ions by Mn-Fe_3O_4-NPs-AC under different experimental conditions.

	Model Parameters	First-order- kinetic			Second-order-kinetic			Intraparticle diffusion			Elovich			
		k_1	$q_{e\ (calc)}$	R^2	k_2	$q_{e\ (calc)}$	R^2	K_{dif}	C	R^2	β	α	R^2	$q_{e\ (exp)}$
MB	0.010 g	0.00990	19.110	0.987	1.071800	100.000	0.999	1.113	78.830	0.994	5.585	3811.010	0.980	97.470
(20 mg L^{-1})	0.015 g	0.00806	10.105	0.924	0.017500	67.560	0.999	0.640	55.420	0.988	3.300	386.720	0.941	66.360
	0.020 g	0.00898	5.670	0.944	0.003600	50.500	0.999	0.336	44.160	0.992	1.746	130.370	0.957	49.920
SO	0.010 g	0.01280	20.860	0.952	0.000121	52.910	0.998	1.033	33.085	0.972	5.495	840.001	0.970	49.960
(10 mg L^{-1})	0.015 g	0.01330	14.880	0.966	0.000412	35.210	0.999	0.736	21.595	0.985	3.663	133.530	0.971	33.300
	0.020 g	0.00967	7.422	0.969	0.000819	25.770	0.998	0.410	17.960	0.994	2.152	49.550	0.983	24.090
Pb^{2+}	0.010 g	0.00806	34.190	0.960	0.000032	158.730	0.996	2.189	116.140	0.976	11.441	7313.023	0.941	153.580
(38 mg L^{-1})	0.015 g	0.00944	28.170	0.979	0.000112	108.690	0.998	1.709	76.343	0.988	9.015	4848.094	0.970	104.850
	0.020 g	0.00783	22.900	0.965	0.000225	87.719	0.997	1.305	61.877	0.986	6.770	4061.621	0.937	85.500
Cr^{3+}	0.010 g	0.00875	34.670	0.962	0.000009	208.330	0.999	1.976	170.480	0.996	10.398	6985.212	0.973	205.150
(42 mg L^{-1})	0.015 g	0.01080	27.580	0.950	0.000028	142.857	0.999	1.358	116.590	0.992	7.129	4383.121	0.965	139.890
	0.020 g	0.01100	15.330	0.957	0.000049	106.380	0.999	0.786	91.046	0.988	4.162	1247.003	0.980	104.920

Table. 5. Isotherm constant parameters and correlation coefficients calculated for the adsorption of dyes and ions onto Mn-Fe_3O_4-NPs-AC in single component system.

		Dye						Ion					
		MB			SO			Cr^{3+}			Pb^{2+}		
Isotherm	Parameters	0.01 g	0.015 g	0.02 g	0.01 g	0.015 g	0.02 g	0.01 g	0.015g	0.02 g	0.01 g	0.015 g	0.02 g
Langmuir	Q_{max}(mg g^{-1})	229.4	121.06	110.86	159.74	111.34	91.99	267.4	165.8	121.65	139.5	123.9	105.2
	K_L (L mg^{-1})	0.929	0.964	2.50	0.677	1.597	1.231	0.949	2.52	1.627	0.848	0.538	0.916
	R^2	0.996	0.994	0.996	0.995	0.996	0.999	0.993	0.999	0.997	0.998	0.999	0.996
	R_L	0.026-0.177	0.025-0.172	0.009-0.074	0.036-0.230	0.015-0.112	0.020-0.140	0.026-0.095	0.009-0.038	0.015-0.058	0.029-0.105	0.044-0.157	0.027-0.098
Freundlich	1/n	0.572	0.385	0.440	0.434	0.410	0.456	0.585	0.513	0.507	0.300	0.444	0.459
	K_F (L mg^{-1})	0.7110	5.520	6.284	5.820	5.720	5.080	8.014	7.980	6.320	6.036	5.078	5.215
	R^2	0.966	0.968	0.905	0.957	0.910	0.940	0.956	0.981	0.985	0.964	0.933	0.973
Temkin	B_1	47.173	20.606	20.62	30.07	21.09	15.78	60.91	36.07	26.34	24.63	26.91	22.71
	K_T(L mg^{-1})	10.940	19.621	37.23	9.345	22.24	18.05	8.797	25.37	16.54	14.96	5.310	9.176
	R^2	0.989	0.987	0.985	0.988	0.961	0.994	0.990	0.996	0.994	0.996	0.991	0.993
Dubinin-radushkevich	Qs (mg g^{-1})	134.30	86.49	80.57	109.4	84.21	66.49	182.8	125.8	87.35	115.1	90.92	77.71
	B×10^{-8}	6.23	4.5	3.2	8.12	4.42	5.3	8.14	3.46	4.65	1.1	9.19	1.8
	E (kJ mol^{-1})	2.833	3.333	3.952	2.500	2.481	3.071	2.478	3.801	3.279	6.742	5.270	2.333
	R^2	0.950	0.893	0.951	0.845	0.894	0.926	0.981	0.979	0.960	0.934	0.943	0.958

856 **Table. 6.** Comparison for the removal of dyes and ions by different methods and adsorbents.

Adsorbent	Dye/ion	Sorption capacity ($mg\ g^{-1}$)	Contact time (min)	Ref.
Platanus orientalis leaves powder (POLP)	MB	114.94	70	63
Gold nanoparticles loaded on activated carbon	MB	185.0	1.6	64
Ag nanoparticles loaded on activated carbon	MB	71.43	15	65
Graphene nanosheet/magnetite (Fe_3O_4) composite	MB	43.83	20	66
magnetite loaded multi-wall carbon nanotube	MB	48.06	120	67
CuO-NP-AC	MB	10.55	15	68
Mn-Fe_3O_4-NPs-AC	MB	229.4	3.0	This work
Mesoporous (MCM-41)	SO	68.8	120	12
Calcined Mussel Shells (CMS)	SO	154.3	60	69
Fe_3O_4-NPs modified with SDS	SO	769.2	10	70
MgO Decked Multi Layered Graphene (MDMLG)	SO	137.6	120	71
NiS-NP-AC	SO	53.2	5.46	30
Mn-Fe_3O_4-NPs-AC	SO	159.7	3.0	This work
Polyacrylamide zirconium(IV) iodate	Pb^{2+}	7.01	60	72
Olive leave powder	Pb^{2+}	119	120	73
Enteromorpha prolifera	Pb^{2+}	134.8	720	74
Phanerochaete chrysosporium	Pb^{2+}	135.3	60	75
Zirconium(IV) iodosulphosalicylate	Pb^{2+}	327.87	120	76
Mn-Fe_3O_4-NPs-AC	Pb^{2+}	139.5	3.0	This work
Graphene oxide	Cr^{3+}	92.65	120	26
Alumina nanoparticles immobilized zeolite	Cr^{3+}	1.82	240	77
Modified Lignin	Cr^{3+}	25	240	78
Bentonite clay	Cr^{3+}	49.75	15	79
Activated alumina powder (AAP)	Cr^{3+}	121.19	50	80
Mn-Fe_3O_4-NPs-AC	Cr^{3+}	267.4	3.0	This work

857
858
859
860
861

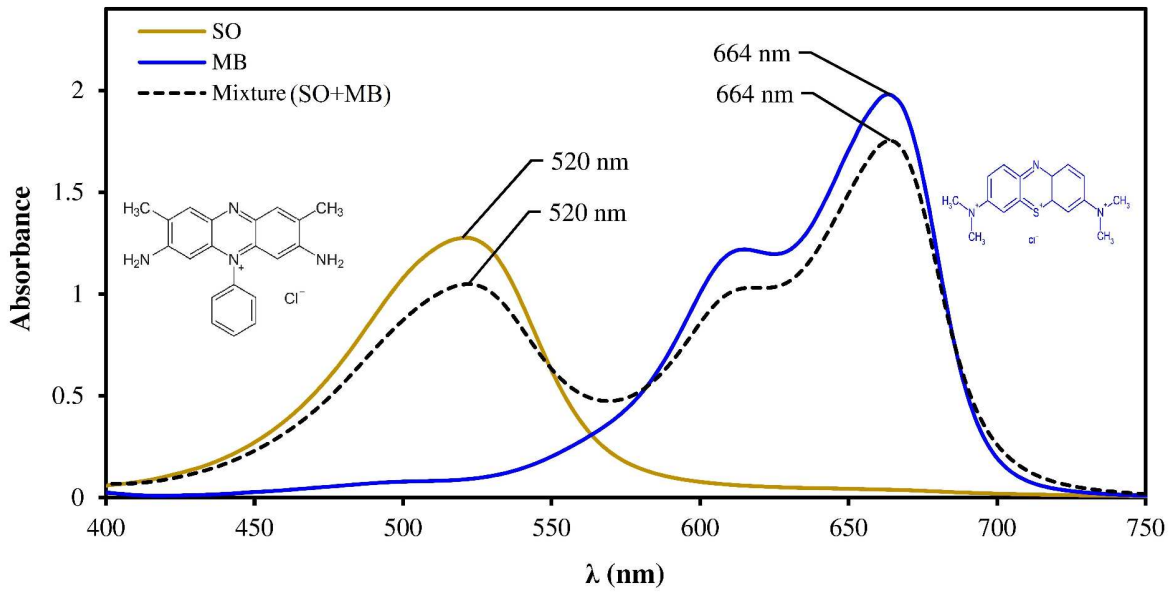

Fig. 1. UV–Vis spectra with chemical structure of MB and SO in single and quaternary solutions (initial dye concentration of 10 mg L^{-1} for each dye and 40 mg L^{-1} for each ion).

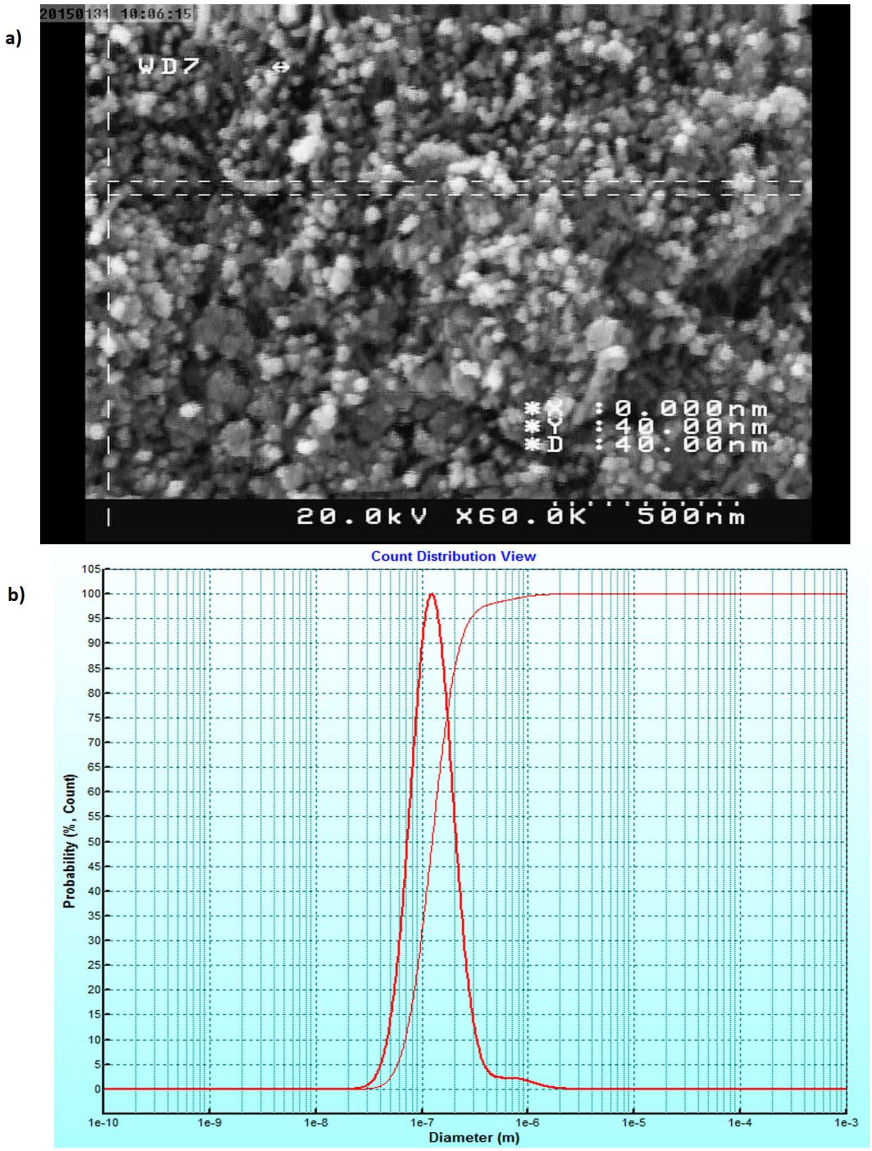

Fig. 2. (a) FE-SEM image of the prepared Mn doped Fe_3O_4-NPs and **(b)** Particle size distribution of the prepared Fe_3O_4 particles.

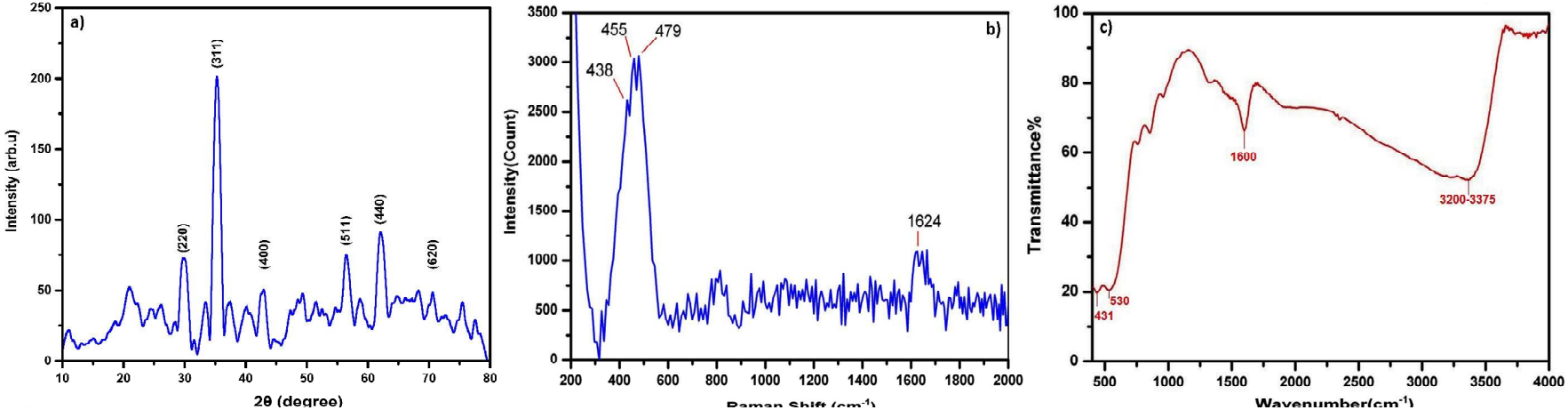

Fig. 3. **(a)** XRD patterns of the prepared Mn doped Fe_3O_4-NPs, **(b)** the Raman spectrum of the prepared Fe_3O_4 particles and **(c)** FT-IR transmittance of the prepared Mn doped Fe_3O_4-NPs.

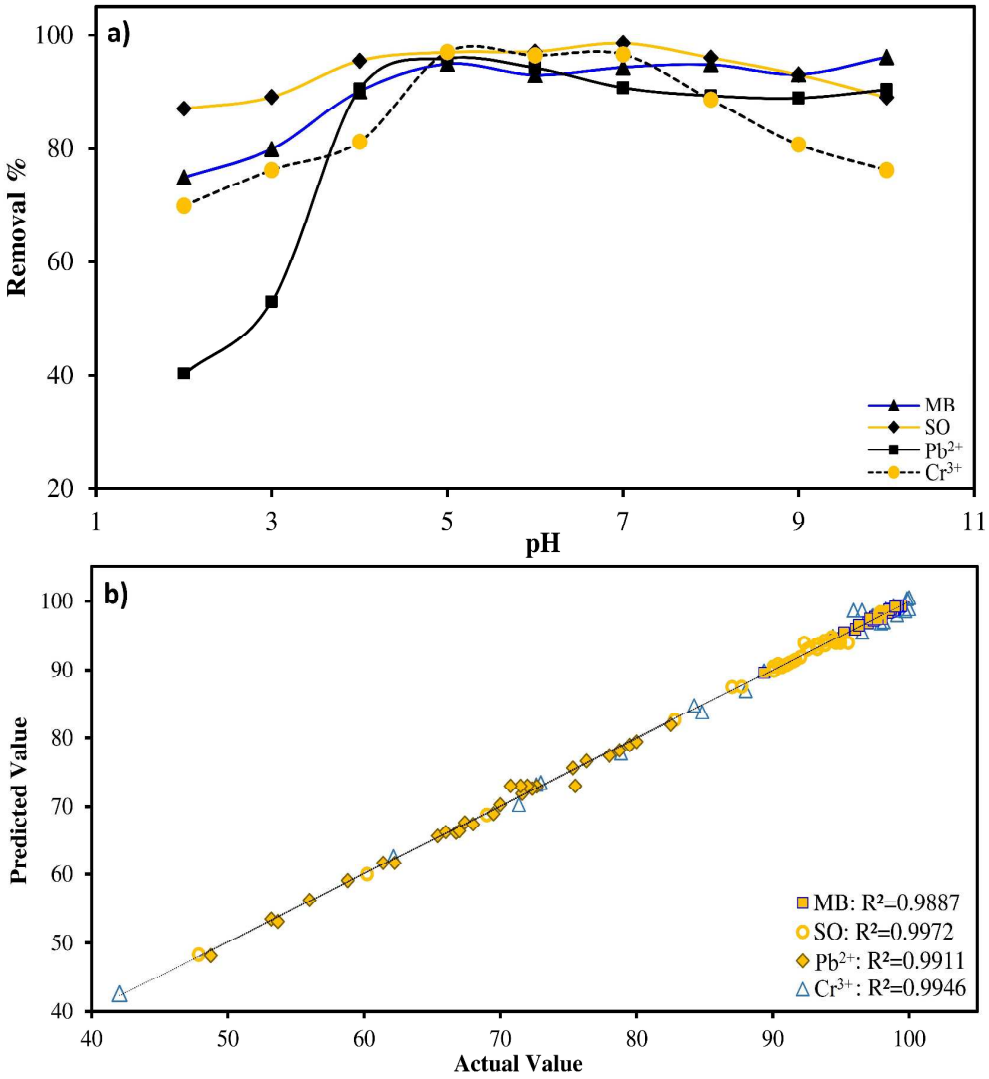

Fig. 4. (a) Effect of pH on the removal of MB, SO, Pb^{2+} and Cr^{3+} in the range of 2.0–10.0. (General condition: adsorbent dose: 0.02 g, ultrasonic time: 4 min, in 50 mL solution, dye concentration: 15 mg L^{-1} for each dye, ion concentration: 40 mg L^{-1} for each ion at room temperature (25 ºC)) and **(b)** the experimental data versus predicted data for removal of MB, SO, Pb^{2+} and Cr^{3+}.

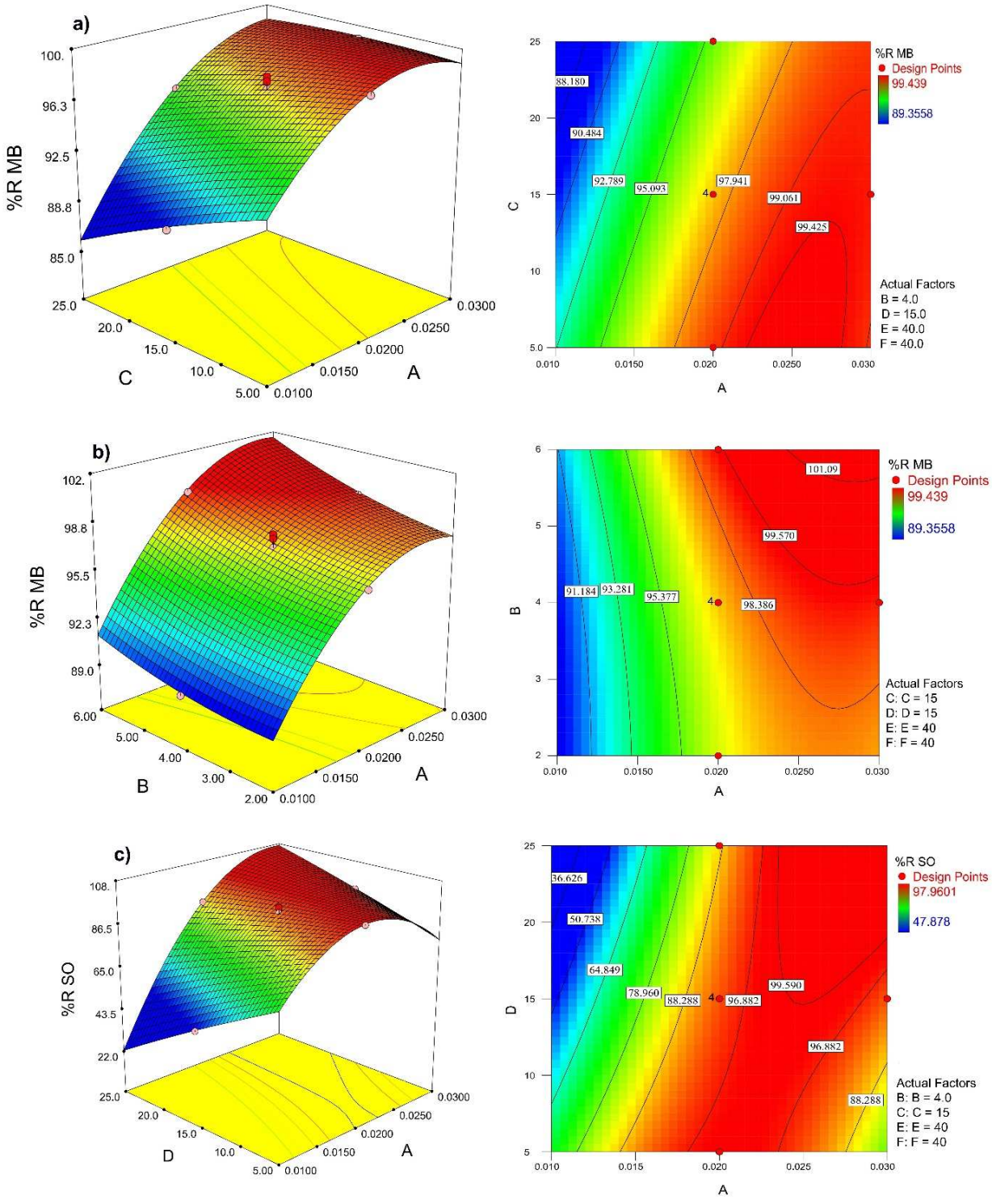

Fig. 5. Response surfaces for the dyes removal **(a)** A-C (MB), **(b)** A-B (MB) and **(c)** A-D (SO).

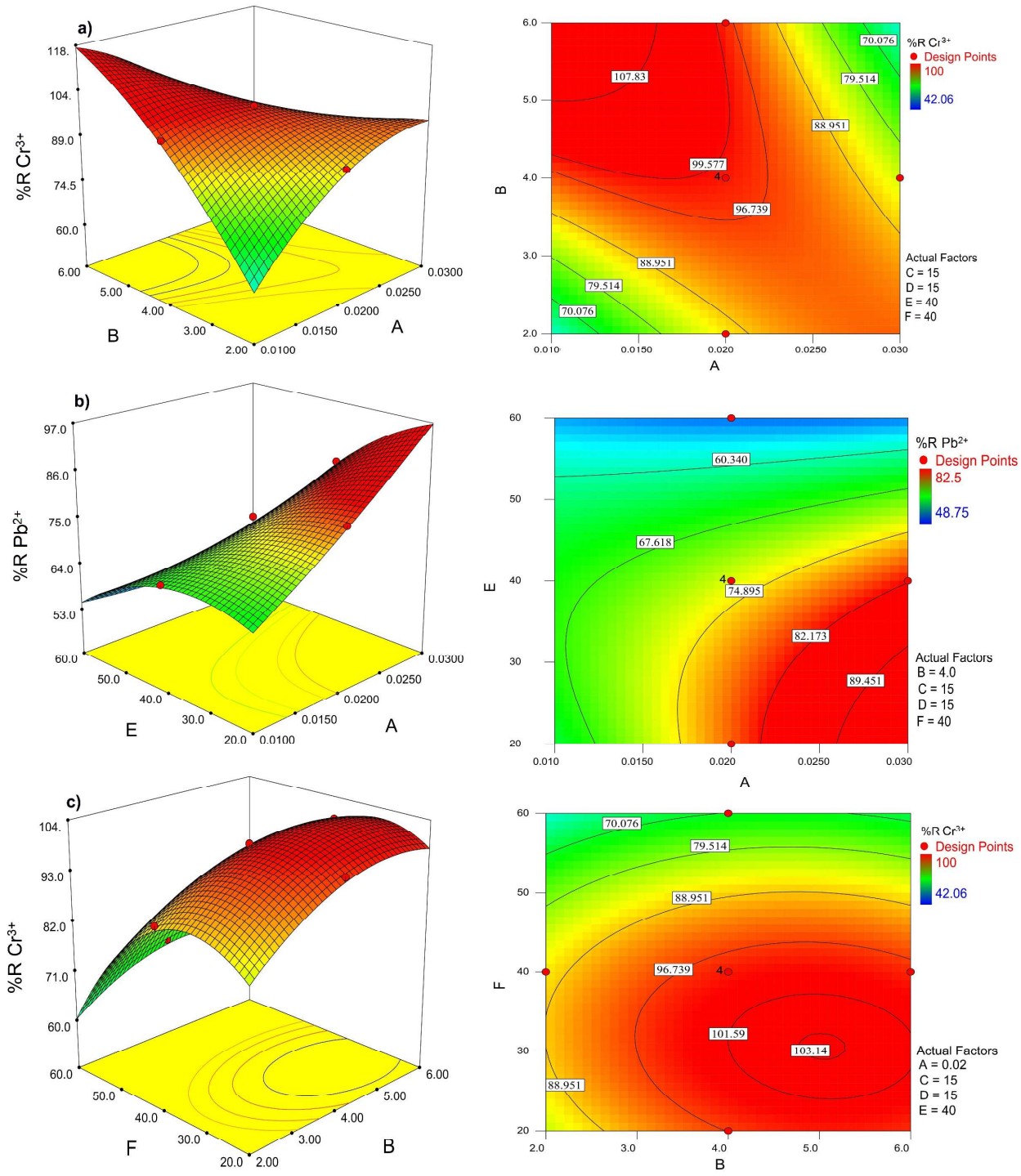

Fig. 6. Response surfaces for the ions removal **(a)** A-B (Cr^{3+}), **(b)** A-E (Pb^{2+}) and **(c)** B-F (Cr^{3+}).

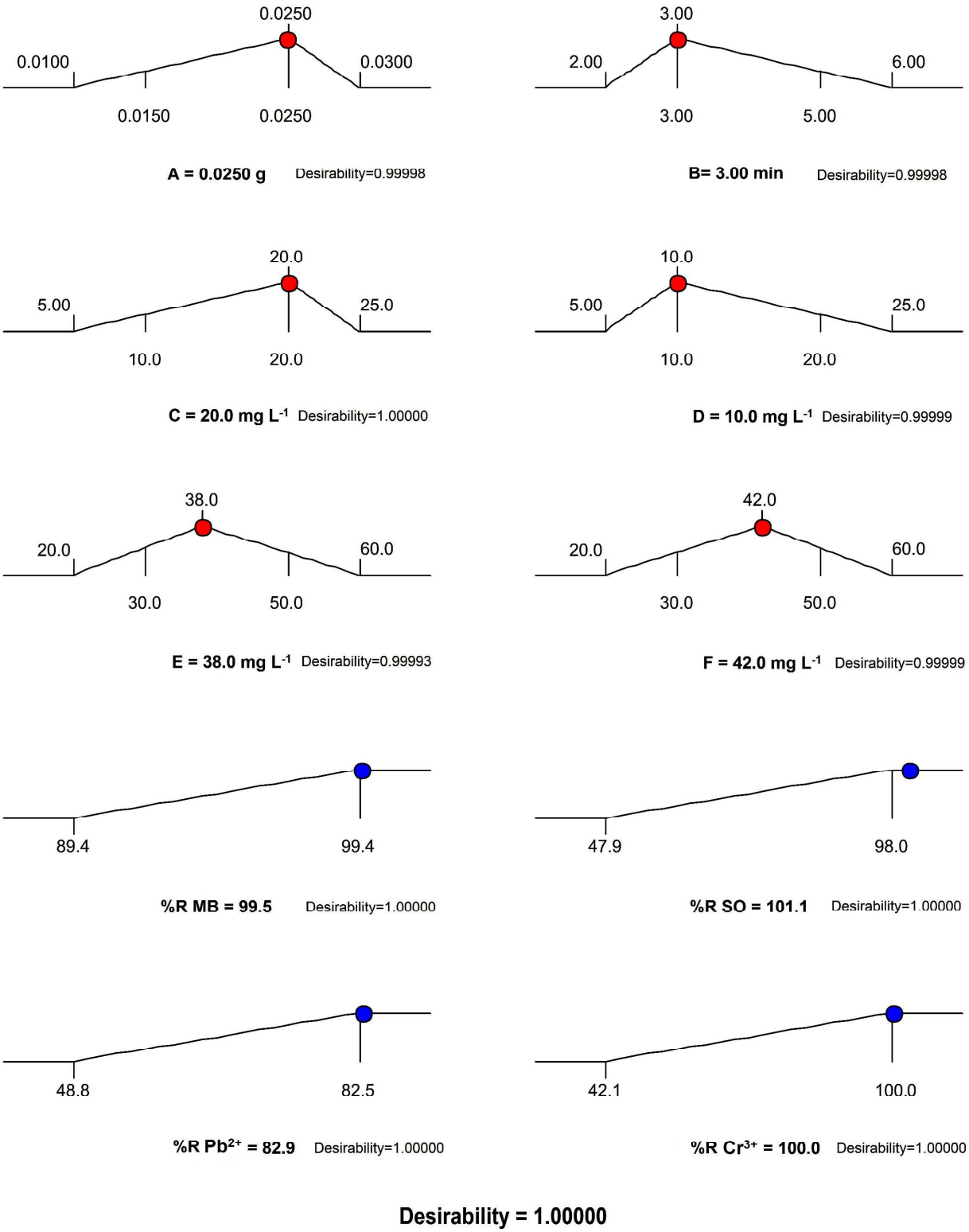

Fig. 7. Profiles for predicated values and desirability function for removal percentage of MB, SO, Pb^{2+} and Cr^{3+}.

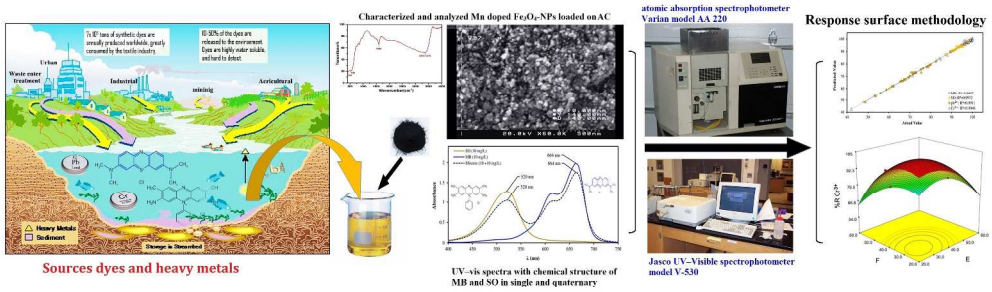

1344x401mm (72 x 72 DPI)